Appl Phys B (2009) 97: 715–722
DOI 10.1007/s00340-009-3636-3

Applied Physics B
Lasers and Optics

Wavelength modulation and cavity enhanced absorption spectroscopy using ∼1.9 μm radiation produced by difference frequency generation with a MgO doped PPLN crystal

M.L. Hamilton · R. Peverall · G.A.D. Ritchie · L.J. Thornton · J.H. van Helden

Received: 20 March 2009 / Revised version: 19 June 2009 / Published online: 17 July 2009

Abstract We have demonstrated the production of ∼1.9 μm near-infrared radiation by using difference frequency generation within a 5% MgO doped PPLN crystal by coupling ∼735 nm radiation from a tunable external cavity diode laser with relatively high powered 532 nm radiation from both Nd:YVO_3 and Nd:YAG lasers. The radiation produced is of low power, ∼15 μW, and was used in conjunction with the sensitivity enhancing techniques of wavelength modulation spectroscopy (WMS) and cavity enhanced absorption spectroscopy (CEAS). Experiments were carried out on rotationally resolved transitions in the combination bands of NH_3 and CO_2 in the 1.9 μm region. An α_{min} value of 3.6×10^{-6} cm^{-1} $Hz^{-1/2}$ was achieved for WMS measurements on CO_2. A comparable α_{min} value of 2.2×10^{-6} cm^{-1} $Hz^{-1/2}$ was achieved for NH_3 using CEAS. The low NIR power indicates that despite the level of MgO doping quoted for the crystal, under prolonged exposure photorefractive damage has occurred.

PACS 33.20.Ea · 42.60.Da · 42.62.Fi · 42.65.Ky · 42.72.Ai, · 42.70.Mp

1 Introduction

Molecular spectroscopy in the near- and mid-infrared regions is highly favourable because of the plethora of molecular fundamental, overtone and combination bands which can be accessed, and therefore selective spectroscopic measurements of a large number of compounds can be made. However, simple narrow linewidth laser sources that cover an appreciable wavelength range ($\gtrsim$200 cm^{-1}) are only generally available in the form of external cavity diode lasers (ECDL) operating at $\lesssim$1.65 μm. Hence there is interest in the production of near- and mid-IR radiation via nonlinear optical processes using widely available sources. The advent of the reliable production of periodically-poled materials for applications in nonlinear optics has opened up wide spectral regions to laser based spectroscopy. The combination of these materials with widely tunable sources, such as ECDLs, enables access to transitions over a relatively large spectral range at high resolution, ($\lesssim$20 MHz) which would represent an advantage for multicomponent trace gas analysis, especially when combined with sensitivity enhancing techniques such as modulation spectroscopy and cavity enhanced methods. Primarily, periodically-poled lithium niobate (PPLN) has been used either in a difference frequency generation (DFG) or optical parametric oscillator arrangement to generate radiation in the mid-IR (3–5 μm) for gas detection applications [1–4].

In this paper, we report preliminary findings limited to the spectral range between 1.9–2 μm and using DFG employing a multi-track 5% MgO doped PPLN crystal with poling periods 8–10.2 μm capable of an extended wavelength coverage 1.8–3 μm with the appropriate pump/signal lasers. If the pump laser is chosen to be at 532 nm, then the signal laser wavelengths will be in the range 645–750 nm; wavelengths which are available from commercial tunable diode lasers. Here, radiation from a tunable ECDL operating at ∼735 nm is mixed with two different relatively high power lasers operating at 532 nm. The resulting near-IR radiation is utilised to probe transitions in the $2\nu_1 + \nu_3$ combination band of carbon dioxide and transitions in the $\nu_3 + \nu_4$ combination band

M.L. Hamilton · R. Peverall (✉) · G.A.D. Ritchie · L.J. Thornton · J.H. van Helden
Department of Chemistry, Physical and Theoretical Chemistry Laboratory, University of Oxford, South Parks Road, Oxford OX1 3QZ, UK
e-mail: robert.peverall@chem.ox.ac.uk
Fax: +44-1865-275410

of ammonia in conjunction with sensitivity enhancing techniques. The techniques used here are cavity enhanced absorption spectroscopy (CEAS), where pathlength enhancement is achieved by use of an optical cavity; and wavelength modulation spectroscopy (WMS) which transfers the detection regime to a higher frequency to reduce technical noise. The performance of these techniques with the relatively low power of near-IR radiation produced, is discussed.

2 Theory

2.1 Difference frequency generation

The induced polarization of a material is dependent upon the applied electric field strength [5]. Typically, with low field strengths this relationship appears linear and only the first order optical susceptibility term needs to be considered. However, when strong fields are applied to the material, such as with laser radiation, higher order optical susceptibility terms become important.

For DFG it is the second-order nonlinear optical susceptibility term which gives rise to the process of interest [5]. In DFG, idler radiation, i, is produced in the crystal by mixing two different radiation sources, the signal, s, and the pump, p. Through conservation of energy, the relationship between the pump, signal and idler radiation frequencies, ω, can be described by: $\omega_p - \omega_s = \omega_i$, where $\omega_p > \omega_s > \omega_i$ by convention. Since nonlinear processes are phase-sensitive, the phase relationship between the pump and signal radiation also needs to be considered. For DFG with collinear beams the phase mismatch is given by

$$\Delta\tilde{k} = \tilde{k}_p - \tilde{k}_s - \tilde{k}_i, \tag{1}$$

where $\tilde{k}_p$, $\tilde{k}_s$ and $\tilde{k}_i$ are the wave vectors of the pump, signal and idler radiation, respectively, and $k_x = (n_x\omega_x)/c$, where n_x is the refractive index of the material at frequency ω_x $(x = i, p, s)$ and c is the speed of light. The efficiency of the DFG process is maximised when $\Delta\tilde{k} = 0$ along the propagation direction of the radiation over the crystal length. To achieve this the configuration of the incident laser beams, the geometry and temperature of the crystal all need to be optimised to ensure a good phase relationship between the interacting beams.

Chromatic dispersion as a consequence of the frequency dependence of the refractive index of a crystal, causes $\Delta\tilde{k}$ to become non-zero. This reduces the efficiency of the nonlinear interaction and results in less idler radiation being produced. To overcome this, quasi-phase matching (QPM) can be used; this is achieved by using periodically-poled materials, such as PPLN, where a periodic change in the local polarity of the second-order optical susceptibility between the layers in the crystal corrects for the phase mismatch. Poling periodically alternates the optical axis, changing the sign of optical susceptibility, allowing efficient generation of the idler radiation. The optimal physical conditions required to maximise the quasi-phase matching in a periodically-poled crystal are achieved when $\Delta k_{\mathrm{QPM}}(T)$ approaches zero,

$$\Delta k_{\mathrm{QPM}}(T) = 2\pi\left(\frac{n_p(T)}{\lambda_p} - \frac{n_s(T)}{\lambda_s} - \frac{n_i(T)}{\lambda_i} - \frac{1}{\Lambda(T)}\right), \tag{2}$$

where λ_p, λ_s and λ_i are the pump, signal and idler wavelength, respectively; $\Lambda(T)$ is the temperature-dependent crystal poling period. Finally, $n_p(T)$, $n_s(T)$ and $n_i(T)$ are the temperature- and wavelength-dependent extraordinary pump, signal and idler refractive indices, respectively, for PPLN as described by the Sellmeier equations [6]. For doped PPLN such as MgO:PPLN, which is used here, the Sellmeier equation requires modification [7], such that

$$n^2_{e,x}(\lambda_x, T) = \left[A_1 + B_1 f(T) + \frac{A_2 + B_2 f(T)}{\lambda_x^2 - (A_3 + B_3 f(T))^2} + \frac{A_4 + B_4 f(T)}{\lambda_x^2 - A_5^2} - A_6\lambda_x^2\right] \Big/ h(T)^2, \tag{3}$$

where λ_x is the wavelength in μm for the i, p and s radiation, and A_z and B_z are the optimised parameters given in Table 1. For undoped PPLN $h(T)$ is unity, but for the MgO:PPLN $h(T)$ is given by

$$h(T) = 1.0270295 - 4.56346827 \times 10^{-5} T, \tag{4}$$

and the temperature parameter, $f(T)$, is defined as

$$f(T) = (T - 24.5) \times (T + 570.5), \tag{5}$$

where T is the crystal temperature in °C.

The experimentally determined temperature tuning curve for the MgO:PPLN crystal is shown in Fig. 1, where the normalised photodiode signal is plotted as a function of crystal oven temperature, also plotted is the expected simulated temperature profile, determined using (2)–(5). An important, but predicted, observation is that the widths of these tuning curves are much narrower than those observed for DFG at longer wavelengths [1]. Due to instabilities in the oven temperature and possible temperature gradients along the crystal the experimentally obtained profile is broadened and detailed structure lost. Furthermore, from the experimental data the optimal temperature for the MgO:PPLN crystal for maximum conversion efficiency is 71°C; this is quite different from the theoretically optimal temperature of 60.4°C; for ease of comparison an x-axis translation has been applied to the theoretical tuning curve in Fig. 1. This indicates that there is a potential uncertainty in the poling period (to which the optimal conversion temperature is very sensitive),

Table 1 The A_z and B_z parameters of the Sellmeier equation for MgO:PPLN

z	1	2	3	4	5	6
A	5.35583	0.100473	0.20692	100	11.34927	1.5334×10^{-2}
B	4.629×10^{-7}	3.862×10^{-8}	-0.89×10^{-8}	2.657×10^{-5}		

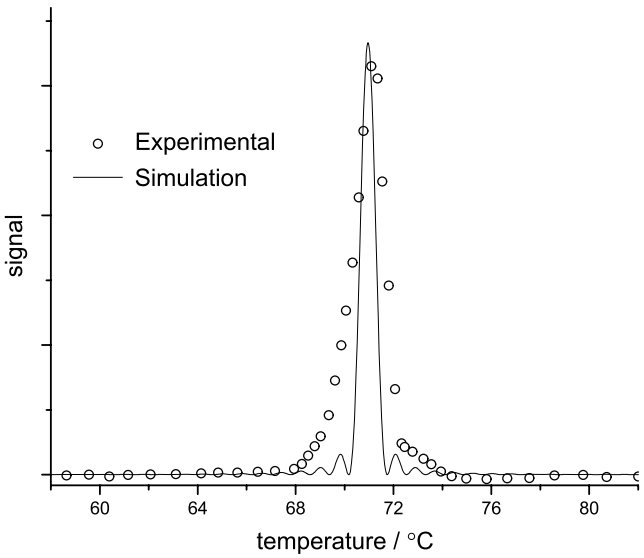

Fig. 1 Temperature tuning curve for MgO:PPLN showing both the experimental and theoretical results, with an x-axis translation applied to the theoretical curve; the reasons for this have been outlined in the text. PPLN was pumped using a DPSS Nd:YAG laser as described in the text

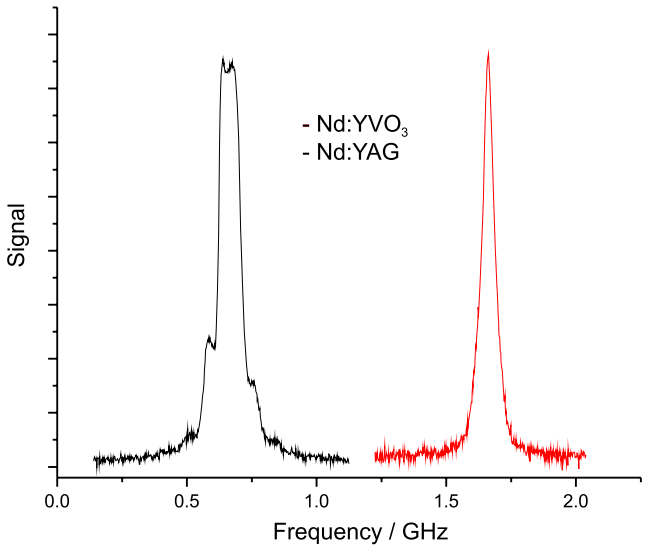

Fig. 2 The 2 GHz optical spectrum analyser traces for the Nd:YAG (*left*) and Nd:YVO_3 (*right*) lasers; clearly shown is the clean single mode behaviour of the Nd:YVO_3 laser compared to the Nd:YAG laser. The quoted bandwidths for both lasers is less than suggested in these traces, and there is some broadening due to the spectrum analyser bandwidth

although some degree of uncertainty in the oven/crystal temperature cannot be ruled out.

Two different diode pumped solid state (DPSS) 532 nm pump lasers of different design, power and optical quality where used in these experiments. One, is an actively temperature stabilised frequency doubled Nd:YAG laser (Quantum Torus) operating at ∼320 mW maximum power and has mode tracking electronics to ensure single longitudinal mode output and a nominal sub-MHz bandwidth. The other is a water cooled, indirectly temperature stabilised Nd:YVO_3 laser (Coherent Verdi V5) which utilises a single longitudinal mode design with a 50 ms bandwidth of <5 MHz and a maximum power output of 5 W. The latter required some warm up time to achieve stability (∼1 hour) but even with a larger stated bandwidth shows higher quality spectral output than the Nd:YAG laser. Figure 2 shows the contrast between the lasers upon analysis using a 2 GHz optical spectrum analyser. The Nd:YAG laser exhibits a less than ideal mode structure with 'sub-modes' growing and receding under an envelope of ∼50 MHz width, while the Nd:YVO_3 laser is truly single mode. The drift in the ∼1.9 μm radiation when using the two different pump lasers was very similar, observed over 20 minutes (10 MHz versus 50 MHz for the Nd:YVO_3 and Nd:YAG, respectively); the major source of drift in this experimental setup is the signal diode laser source (∼400 MHz over the same 20 min measurement period).

2.2 Absorption spectroscopy

Two different spectroscopic techniques were used to increase the experimental sensitivity over single-pass direct absorption spectroscopy. Presented here is a brief outline on how these techniques work and how the enhanced sensitivity is achieved; more comprehensive descriptions can be found elsewhere [8–10].

The first method, CEAS, exploits the enhancement in the effective pathlength that the radiation travels by the use of an optical cavity, where the radiation is trapped between two highly reflective mirrors [8, 10].

The simplest optical cavity consists of two mirrors with radii of curvature r_1 and r_2 and reflectivity R in a linear arrangement. Radiation is coupled into the cavity through the backface of the first mirror and is then trapped between the two reflective faces of the mirrors. A detector placed behind the second mirror is used to detect the time-integrated

radiation intensity as the laser is scanned across the spectral region of interest. The intensity profile *versus* frequency of the radiation detected is dependent on the cavity mirror separation, the precise geometry of the cavity with respect to the optical axis, laser power and mirror reflectivity and transmission. To optimise CEAS the mirrors are partially misaligned so as to optimise the mode density and re-entrant condition of the cavity, hence sequential scans can be averaged to give a smooth spectrum which can be described by

$$\frac{I_0(\nu) - I(\nu)}{I(\nu) - \gamma} = \frac{\sigma(\nu)cl}{1 - R}, \tag{6}$$

where $I_0(\nu)$ is the baseline signal, $I(\nu)$ is the recorded signal with the sample present, l is the cavity length, γ is comprised of any background signal, R is the geometric mean of the reflectivity of the cavity mirrors and $\sigma(\nu)$ is frequency-dependent absorption cross section of the absorbing medium and c is its concentration.

The second technique employed is WMS, in which the absorption signal is moved to a higher frequency domain where technical noise sources are less likely to interfere with the signal. Experimentally, WMS involves rapid modulation of the wavelength of the laser as it slowly traverses the spectral feature of interest. Hence there are two frequency components which require definition, ω_L known as the central laser frequency which is slowly ramped and traverses the absorption profile and ω_m which is the rapid modulation superimposed on ω_L, its amplitude ($\Delta\omega_m$) is usually experimentally optimised and is generally similar to the halfwidth of the spectral feature being investigated [11]. The overall instantaneous angular frequency of the electric field of the laser, ω, which is the combination of both of the above frequency components is described by

$$\omega = \omega_L + \Delta\omega_m \cos(\omega_m t). \tag{7}$$

The interaction between absorbing species and the spectrally modulated light leads to changes in the time-dependent intensity of the modulated radiation. This can be expressed as a cosine Fourier series,

$$I(\omega_L, t) = \sum_{n=0}^{\infty} A_n(\omega_L) \cos(n\omega_m t), \tag{8}$$

where $A_n(\omega_L)$ (where $n > 0$) are the harmonic components of the series. To record a WMS spectrum the detector signal is demodulated, generally by a lock-in amplifier. Any noise contributions that do not coincide with the modulation frequency are essentially not detected. Assuming that I_0 is independent of frequency in the absence of an absorber, and by substituting $\omega_m t$ with θ, each individual harmonic component in the presence of a frequency-dependent absorption cross section $\sigma(\omega)$, is given by

$$\begin{aligned} A_n(\omega_L) &= \frac{2}{\pi} \int_0^{\pi} I_0(\omega_L + \Delta\omega_m \cos\theta) \\ &\quad \times \exp\left[-\sigma(\omega_L + \Delta\omega_m \cos\theta)cl\right] \cos(n\theta)\, \mathrm{d}\theta \\ &= \frac{2I_0}{\pi} \int_0^{\pi} \exp\left[-\sigma(\omega_L + \Delta\omega_m \cos\theta)cl\right] \cos(n\theta)\, \mathrm{d}\theta. \end{aligned} \tag{9}$$

In the limit of low absorbance when $\sigma cl \ll 1$, the expression simplifies to

$$A_n(\omega_L) = \frac{2I_0 cl}{\pi} \int_0^{\pi} -\sigma(\omega_L + \Delta\omega_m \cos\theta) \cos(n\theta)\, \mathrm{d}\theta. \tag{10}$$

Although WMS is good for removing noise, the WMS spectrum obtained is not self-calibrating, unlike single-pass direct absorption spectroscopy. To determine absolute concentrations calibration against single-pass direct absorption spectroscopy or measurements of standard gas mixtures is generally required, although a recent publication suggests that WMS spectra may be calibrated directly from the residual amplitude modulation (RAM) signal [12].

3 Experimental

A schematic of the DFG experimental setup is depicted in Fig. 3 and is common to both CEAS and WMS experiments. The pump beam was provided by one of two different DPSS lasers at 532 nm (Coherent Verdi V5, ~800 mW and Quantum Torus, 320 mW) and the ECDL operating at ~735 nm (Sacher Lynx, ~40 mW) provided the signal; polarisation matching to the pump beam was achieved using a half waveplate. To protect the diode laser from optical feedback the beam was passed through an optical isolator (Isowave 1-7090-CM). A spectrum analyser (Melles Griot), with a free spectral range of 2 GHz, was used for wavelength calibration and to monitor the behaviour of the diode laser. Wavelength tuning of the system was possible by temperature and current tuning of the diode laser. Tuning the diode laser to 737 and 732 nm generated the necessary idler radiations at 1.91 and 1.95 μm, respectively. The pump and signal beams were combined using a dichroic mirror, and focusing lenses prior to the dichroic mirror focused the beams into the 5% MgO:PPLN crystal. The MgO:PPLN crystal (HC Photonics, 40 × 14.5 × 0.5 mm) is AR coated for 532 and 640–750 nm and has 12 tracks with poling periods ranging from 8.0–10.2 μm, of which the 8.2 μm track was used for this work. The crystal was situated inside an HC Photonics oven, which was optimally aligned using a three-axis micrometer stage. The oven temperature was set to maximise the crystal's conversion efficiency and was 72.5°C and 109°C to produce the 1.91 and 1.95 μm radiation, respectively. The three

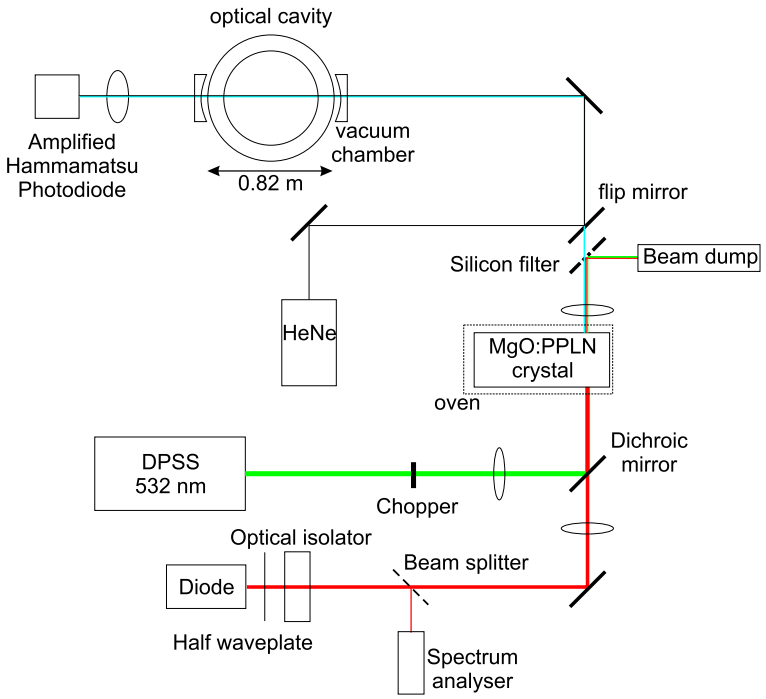

Fig. 3 Schematic of the DFG experimental setup used for CEAS measurements of NH_3 at 1.91 μm. For the direct absorption and WMS experiments carried out on CO_2 and NH_3 at 1.95 μm the vacuum chamber was replaced with a 10 cm glass cell

beams exiting the crystal were separated using a silicon filter; the ∼1.9 μm radiation was transmitted whereas the visible beams were reflected into a beam dump. The ∼1.9 μm radiation was collimated using a 10 cm focal length lens and passed through either the CEAS setup incorporated into the vacuum chamber (shown in Fig. 3) or through a 10 cm glass cell; it was then focused onto an amplified photodiode (Hammamatsu G5852-01). With pump and signal powers of 300 mW and 20 mW, respectively, approximately 15 μW of ∼1.9 μm was generated in the crystal, although after losses due to optics only ∼4 μW was incident upon the cavity or glass cell. To aid in alignment the path of the ∼1.9 μm beam was tracked by a HeNe alignment laser (Fig. 3).

The power output of the system is much lower than theoretical calculations predict [13], and we have achieved a maximum efficiency for the DFG here of ∼0.25% using the Nd:YAG laser; we suspect that this is due to photorefractive damage to the crystal. This was affirmed when using the higher power laser: as the pump was increased, the near IR power (∼1.9 μm) would only temporarily increase before dropping back to approximately the original levels. There seems to be a relatively large variation of reported damage thresholds for MgO:PPLN (congruent form) in the literature (doping concentrations similar to this crystal), with values ranging from 10 kW cm^{-2} to 75 kW cm^{-2} [14–17]. We estimate that we have maximum intensities between 25 kW cm^{-2} and 80 kW cm^{-2}, but we also note that damage threshold experiments are reported for relatively short exposure times ∼10 minutes not for extended use near threshold values over a number of hours [14, 15].

During single-pass direct absorption measurements on CO_2 and NH_3 at 1.95 μm a triangular ramp, to scan the laser ∼3.4 GHz (ramped at 10 Hz), was applied to the piezoelectric transducer of the diode laser grating element using a function generator (TTi TG330). The 532 nm beam was also modulated using an optical chopper (Bentham, ∼1 kHz). The 1.95 μm radiation was passed through the glass sample cell and the detector signal was then demodulated using the lock-in amplifier (Stanford Research Systems, SR510) before being displayed on the oscilloscope (LeCroy WaveSurfer 434); 50 averages were taken for each spectrum. Due to the slightly improved linewidth and stability achievable with the Nd:YVO_3 laser, all the spectroscopic measurements reported here have been recorded using this laser.

WMS was conducted by applying a low ramping frequency, ω_0 (over ∼3.4 GHz ramped at ∼2.5 Hz) to the laser in a similar fashion as for single-pass direct absorption. The reference output of the lock-in amplifier was used to produce the fast sinusoidal modulation frequency, ω_m, ∼1.4 kHz with a modulation depth, $\Delta\omega_m$, of ∼300 MHz. The radiation was passed through the glass sample cell and the spectra were collected in a similar fashion as for single-pass direct absorption, again 50 averages were taken. Although $1f$-harmonic detection gave larger signal amplitudes, $2f$-harmonic detection was used throughout these experiments to reduce baseline variation.

Finally, a CEAS setup shown in Fig. 3, was implemented at 1.91 μm to make measurements on NH_3 using selected rotational transitions within the $(\nu_3 + \nu_4)$ band. During these

measurements the pump beam was modulated using an optical chopper (∼1 kHz) and the detector signal demodulated using the lock-in amplifier. A slow laser scanning speed (3.7 mHz) was required because of the long time constant needed by the lock-in amplifier which was essential in order to detect the very low powers after the cavity; input power resident on the cavity was only ∼4 μW, hence the output power is likely to be only tens of pW. The cavity length as dictated by the width of the vacuum chamber was 82 cm. The cavity mirrors were mounted in gimbal mounts onto the vacuum chamber and their reflectively, R, was experimentally determined to be 0.9993, using an NH_3 sample of known concentration.

4 Results and discussion

Single-pass direct absorption profiles of CO_2 and NH_3 at 1.95 μm were fitted with Voigt lineshapes. Generally low pressure spectra are fitted with Gaussian profiles as the major line-broadening component is Doppler broadening (characterised by a FWHM, $\Delta\nu_D$). As gas pressures increase there is also a self-broadening component with a Lorentzian line shape (characterised by a FWHM, $\Delta\nu_L$). Pure samples of CO_2 and NH_3 with pressures between 2–10 Torr were prepared for the WMS experiments, hence the collected spectra were expected to contain only a small self-broadening component.

Table 2 contains the details of the transitions probed such as line positions and integrated cross sections along with broadening parameters obtained from the HITRAN 2004 database [18]. The Doppler widths for a sample temperature of 296 K are also tabulated. The expected DFG idler radiation bandwidth is <10 MHz which is sufficiently high resolution to easily resolve the Doppler broadening of ∼300 MHz.

The areas of the fitted Voigt profiles of the absorption spectra were used to accurately determine the sample gas pressures and to calibrate the WMS spectra. The resulting pressures were 8.3 and 2.1 Torr for CO_2 and NH_3, respectively.

The experimental WMS profiles for CO_2 and NH_3 are plotted in Fig. 4, also shown are simulations calculated using a MATLAB program. The $\Delta\nu_D$ and $\Delta\nu_L$ parameters from the fitting of the WMS spectra are reported in Table 3 and are in good agreement with calculated values, the associated error values have been determined as a combination of the errors in the fitting of the direct absorption profiles and the x-scale calculation.

The sensitivity of the WMS setup can be described by an $\alpha_{\min}$ value, corrected for the effective bandwidth of the detection system,

$$\alpha_{\min}(BW_{\text{eff}}) = \frac{abs}{lS/N}\sqrt{\pi\tau n}, \tag{11}$$

where S/N is the signal to noise ratio of the WMS signal, where the noise is defined as twice the standard deviation of baseline variations; abs is the peak absorbance; l is the cell length, τ is the lock-in amplifier time constant and n is the number of averages. The $\alpha_{\min}$ values are independent of sample and a value of 3.6×10^{-6} cm^{-1} Hz$^{-1/2}$ was achieved for this experimental setup from the CO_2 data, Fig. 4.

CEAS measurements were carried out on 50 mTorr of NH_3 using 1.91 μm radiation. Due to the low power of the laser radiation incident on the cavity the signal collected by the detector was very small. Therefore to get a significant signal to noise ratio which allowed for reliable analysis, the time constant on the lock-in amplifier needed to be longer than that which is typically used in this type of CEAS experiment. The drawback of longer time constants is that they require the system to be stable over an extended period, consequently, any drifting of the laser or related components results in reduced performance and possible broadening of the absorption profile. The time constant used for these measurements was 3 s; longer time constants where investigated which resulted in improvements in signal to noise ratio but also broadened profiles.

The CEAS spectrum for a single scan and the corresponding Gaussian fit are shown in Fig. 5; the experimental $\Delta\nu_D$ of 0.016 ± 0.002 cm^{-1} was obtained by analysing each of the spectra individually and then averaging the fitting results; averaging prior to analysis was not carried out due to setup instabilities which resulted in baseline fluctuations and spectral feature drifts. The calculated value of $\Delta\nu_D$, 0.0156 cm^{-1} (Table 2), is within experimental error. The

Table 2 Transition information for the CO_2 and NH_3 lines of interest, where the transition assignments are presented as $\Delta J\, J''$ for CO_2 and ${}^{\Delta k}\Delta J\,(J'', k'')$(sym) for NH_3

	Line position cm^{-1} (μm)	Assignment	Integrated cross section cm^{-1}/(molecules cm^{-2})	Self-broadening coefficient cm^{-1}/atm	$\Delta\nu_D$ cm^{-1}
CO_2–WMS	5123.586 (1.91)	$R34$	1.521×10^{-21}	0.0835	0.00951
NH_3–WMS	5123.645 (1.91)	${}^{R}R(5,4)$(s)	3.468×10^{-21}	0.5653	0.0153
NH_3–CEAS	5234.482 (1.95)	${}^{P}R(6,5)$(s)	1.22×10^{-22}	0.5755	0.0156

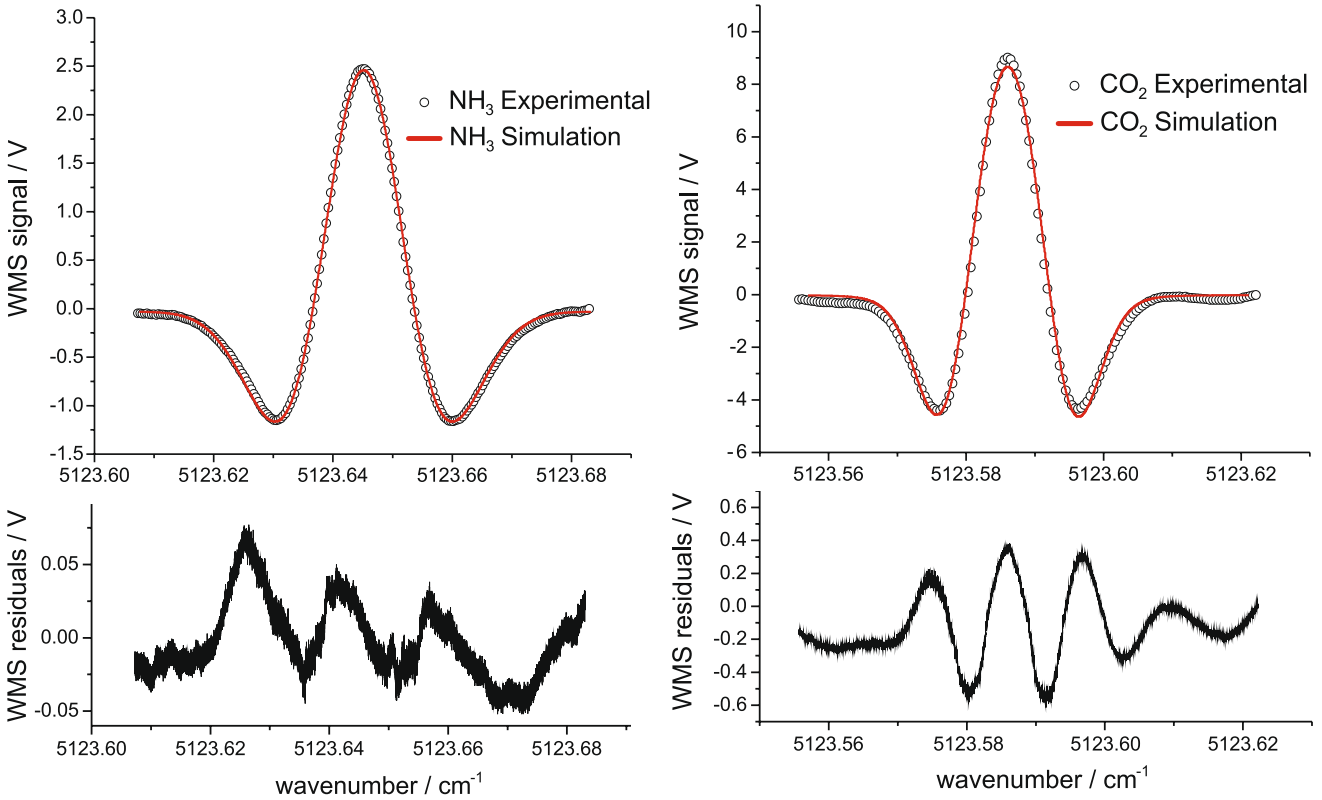

Fig. 4 WMS spectra for CO_2 and NH_3 at 8.3 and 2.1 Torr, respectively, also shown are the fitted Voigt profiles. The lower plots for each show the residuals for each fit; these highlight a slight asymmetry in the experimental data. This is possibly due to the lock-in detection

Table 3 Theoretical and experimental Doppler and Lorentzian FWHM values

	Doppler width, $\Delta\nu_D$/296 K			Lorentzian width, $\Delta\nu_L$		
	Theory	Direct absorption error 3%	WMS error 3%	Theory	Direct absorption error 6%	WMS error 6%
CO_2	0.00952	0.0108	0.00857	0.0018	0.0013	0.0017
NH_3	0.0153	0.0157	0.0153	0.0031	0.0036	0.0039

improvement in sensitivity over WMS is apparent through a decrease in the $\alpha_{\min}$ value to 2.2×10^{-6} cm^{-1} Hz$^{-1/2}$, determined using

$$\alpha_{\min}(BW_{\text{eff}}) = \frac{(1-R)2SD}{l}\sqrt{\pi\tau n}, \tag{12}$$

where R is the mirror reflectivity and SD is the standard deviation of the baseline noise. It is clear that, although there is a slight improvement in sensitivity for the CEAS experiment, at these power levels this is not significant enough to counter the difficulties in implementation. Nevertheless, the 2σ $\alpha_{\min}$ values reported here are not unreasonable for mirrors of reflectivity $R \sim 99.93\%$ and compared to experiments using higher power sources ($\sim$10 mW) with sensitivities $\sim 10^{-8}$ cm^{-1} [8, 10].

5 Conclusion

The production of near-IR radiation has been successfully achieved by combining 532 nm radiation from either a Nd:YAG or a Nd:YVO_3 laser with 732/737 nm radiation from an ECDL in a MgO:PPLN crystal. The resultant $\sim$1.9 μm radiation has been used in both WMS and CEAS experiments to achieve relatively high sensitivities while retaining accurate spectral information in the form of linewidths.

Both WMS and CEAS yielded minimum absorption coefficients in the range 2–4 $\times$ 10^{-6} cm^{-1} Hz$^{-1/2}$ and although there is a slight improvement in the $\alpha_{\min}$ value for CEAS, there is no real benefit over WMS since the low light levels make the alignment and data acquisition difficult and time consuming. Unfortunately, the crystal used in

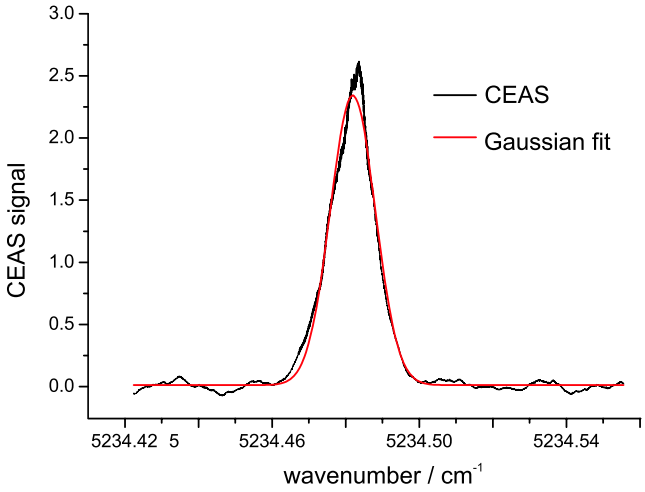

Fig. 5 CEAS spectrum of 50 mTorr of NH_3; also shown is a Gaussian fit

these studies has suffered damage, probably photorefractive, as a consequence of laser intensities utilised here. Even with the lower power Nd:YAG laser at 300 mW, and although reported damage thresholds for congruent lithium niobate with ∼5% MgO doping can be as high as 75 kW cm^{-2} over a relatively short timescale (hours), damage has occurred (we estimate this is ∼3 times greater than intensities applied to the crystal using the Nd:YAG laser). MgO doped stoichiometric PPLN has a much higher damage threshold and is a more suitable material for high power DFG [15, 17].

Acknowledgements The authors gratefully acknowledge the Royal Society for the award of University Research Fellowship to G.A.D.R., and we thank the EPSRC for financial support and an advanced fellowship R.P. The authors gratefully acknowledge helpful discussions with Professor G. Hancock.

References

1. H.Y. Clark, L. Corner, W. Denzer, G. Hancock, A. Hutchinson, M. Islam, R. Peverall, G.A.D. Ritchie, Chem. Phys. Lett. **399**, 102 (2004)
2. W.D. Chen, J. Cousin, E. Poullet, J. Burie, D. Boucher, X.M. Gao, M.W. Sigrist, F.K. Tittel, C. R. Phys. **8**, 1129–1150 (2007)
3. G. D'Amico, G. Pesce, G. Rusciano, A. Sasso, Opt. Lasers Eng. **37**, 481 (2002)
4. O. Tadanaga, T. Yanagawa, Y. Nishida, H. Miyazawa, K. Magari, M. Asobe, H. Suzuki, Appl. Phys. Lett. **88**(6) (2006)
5. R.W. Boyd, *Nonlinear Optics*, 2nd edn. (Academic Press, San Diego, 2003)
6. D.H. Jundt, Opt. Lett. **22**, 1553 (1997)
7. HC Photonics, *HC Photonics, MgO:PPLN specifications*, Hsinchu 300, Taiwan, http://www.hcphotonics.com/ppxx.htm
8. M. Mazurenka, A.J. Orr-Ewing, R. Peverall, G.A.D. Ritchie, Annu. Rep. Prog. Chem., Sect. C Phys. Chem. **101**, 100 (2005)
9. J.M. Supplee, E.A. Whittaker, W. Lenth, Appl. Opt. **33**, 6294 (1994)
10. G. Berden, R. Peeters, G. Meijer, Int. Rev. Phys. Chem. **19**(4), 565–607 (2000)
11. A. Hutchinson, *Diode laser studies of trace species and their reactions*. Doctor of philosophy, University of Oxford (2006)
12. K. Duffin, A.J. McGettrick, W. Johnstone, G. Stewart, D.G. Moodie, J. Lightwave Technol. **25**(10), 3114–3125 (2007)
13. S. Borri, P. Cancio, P. De Natale, G. Giusfredi, D. Mazzotti, F. Tamassia, Appl. Phys., B Lasers Opt. **76**(4), 473–477 (2003)
14. Y. Furukawa, K. Kitamura, A. Alexandrovski, R.K. Route, M.M. Fejer, G. Foulon, Appl. Phys. Lett. **78**(14), 1970–1972 (2001)
15. Y. Furukawa, K. Kitamura, S. Takekawa, A. Miyamoto, M. Terao, N. Suda, Appl. Phys. Lett. **77**(16), 2494–2496 (2000)
16. Y.L. Chen, J. Guo, C.B. Lou, J.W. Yuan, W.L. Zhang, S.L. Chen, Z.H. Huang, G.Y. Zhang, J. Cryst. Growth **263**(1–4), 427–430 (2004)
17. S. Chen, H. Liu, Y. Kong, Z. Huang, J. Xu, G. Zhang, Opt. Mater. **29**, 885–888 (2007)
18. L.S. Rothman, D. Jacquemart, A. Barbe, D.C. Benner, M. Birk, L.R. Brown, M.R. Carleer, C. Chackerian, K. Chance, L.H. Coudert, V. Dana, V.M. Devi, J.M. Flaud, R.R. Gamache, A. Goldman, J.M. Hartmann, K.W. Jucks, A.G. Maki, J.Y. Mandin, S.T. Massie, J. Orphal, A. Perrin, C.P. Rinsland, M.A.H. Smith, J. Tennyson, R.N. Tolchenov, R.A. Toth, J. Vander Auwera, P. Varanasi, G. Wagner, J. Quant. Spectrosc. Radiat. Transfer **96**, 139 (2005)